Journal of ELECTRONIC MATERIALS, Vol. 44, No. 11, 2015
DOI: 10.1007/s11664-015-3951-x

Polarization-Independent, Thin, Broadband Metamaterial Absorber Using Double-Circle Rings Loaded with Lumped Resistances

JUNFENG CHEN,[1,4] XIUTAO HUANG,[2] GEBRU ZERIHUN,[2] ZHAOYANG HU,[1] SHENGMING WANG,[1] GUODONG WANG,[3] XIWEI HU,[1] and MINGHAI LIU[1,5]

1.—State Key Laboratory of Advanced Electromagnetic Engineering and Technology, Huazhong University of Science and Technology, Wuhan 430074, China. 2.— School of Physics, Huazhong University of Science and Technology, Wuhan 430074, China. 3.— Kuang-Chi Institute of Advanced Technology, Shenzhen 518057, China. 4.—e-mail: jfchen@hust.edu.cn. 5.—e-mail: mhliu@mail.hust.edu.cn

We present a broadband and polarization-insensitive metamaterial absorber (MA) composed of a dielectric substrate sandwiched with double-circle rings (DCRs) and welded with lumped resistances and continuous metal film. The structure is designed with thickness of 3 mm and investigated by simulation, fabrication, and experiment. The results show that the composite MA loaded with lumped resistances has wider absorptivity compared with a structure with only DCRs. The simulation results indicate that the proposed absorber achieves 7.60-GHz-wide absorption from 8.87 GHz to 16.47 GHz with absorptivity greater than 90%, in excellent agreement with experimental results. Further simulations indicate that there exist optimal values for the lumped resistances for which the absorptivity is the highest and the bandwidth widest. Additionally, the proposed MA is polarization insensitive at normal incidence. Simulation results for wide angles of incidence of both transverse electric and transverse magnetic waves are also investigated.

Key words: Metamaterial absorber, broadband, polarization insensitive, thin, lumped resistances

INTRODUCTION

Over the past several years, electromagnetic (EM) metamaterials have sparked much interest due to their excellent EM properties. Many exotic EM properties of metamaterials have been demonstrated and applied in many fields such as for invisibility cloaks, wireless power transfer, metamaterial antennas, and perfect MAs. The concept of a perfect MA was first proposed by Landy et al.[1] in the microwave region. The proposed absorber had an ultrathin structure and near-unity absorption at 11.5 GHz. Subsequently, many researchers studied such microwave absorbers to achieve multiband,[2,3] polarization-insensitive,[4,5] wide-incidence-angle,[6,7] and tunable absorption.[8] However, the high absorption of MAs is generally based on their nature of resonance response, so the working bandwidth is relatively narrow.

To increase the absorption bandwidth, researchers have proposed several methods such as use of a multilayer structure,[9] magnetic medium,[10,11] resistive film,[12–14] and loading with lumped elements.[15,16] To date, all these methods are still not particularly easy to implement. In addition, some methods to achieve broadband absorption result in undesirable structural weaknesses; For example, multilayer broadband MAs have high thickness and are difficult to fabricate, limiting their practical applications. Broadband MAs based on magnetic media have increased weight and insufficiently wide absorption bandwidth.

(Received March 31, 2015; accepted July 21, 2015; published online August 11, 2015)

In this work, we numerically and experimentally investigated the absorption rates of a broadband MA consisting of a simple periodic array of DCRs loaded with lumped resistances and a continuous metal film separated by a dielectric substrate. Simulation and experimental results are presented together with a theoretical explanation of the broadband absorption. Moreover, based on the high geometric symmetry of the circle rings, the absorption rates of the proposed MA are also analyzed for different incidence angles and polarizations.

NUMERICAL AND EXPERIMENTAL DEMONSTRATION

The double-circle rings MA (DCR-MA) was designed and optimized based on a simple circle ring structure using CST Microwave Studio. Figure 1a shows a schematic diagram and the geometric parameters of the DCR-MA unit cell with axes indicating the polarization and propagation directions of the incident wave. Periodic boundary conditions are applied along the lateral directions of the DCR-MA, and open boundary conditions along the wave propagation direction. A lossy FR-4 substrate with relative permittivity $\varepsilon_r = 4.0$ and loss tangent $\tan\delta = 0.025$ is used. The metallic material is copper with electrical conductivity $\sigma = 5.8 \times 10^7$ S/m and thickness $t = 0.035$ mm. The final optimized geometry of the unit cell is given by: $a = 14$ mm, $d = 3$ mm, $r_1 = 5.2$ mm, $r_2 = 3.9$ mm, $g = 1.6$ mm, $w_1 = 0.2$ mm, and $w_2 = 0.5$ mm. The outer and inner ring resistances were selected as $R_1 = 470\,\Omega$ and $R_2 = 1000\,\Omega$, respectively. Due to the shielding by the copper film, the transmission is zero for all frequency ranges, thus reflection is the only factor determining the absorption. Therefore, the absorption rate can be calculated as $A(\omega) = 1 - R(\omega) = 1 - |S_{11}|^2$, where S_{11} is the reflection coefficient. Both the electric and magnetic resonances can be excited independently, confining the EM power to the DCR-MA cell. The EM power will gradually be absorbed by conduction, dielectric, and resistance losses.

The resonant behavior can be described by an equivalent inductance (L) and capacitance (C) circuit structure. Langley et al.[17,18] reported using an equivalent circuit model for a periodic array of double loops consisting of the parallel connection of two LC series circuits. However, that model is only valid for a free-standing structure. The series capacitance should include the contribution from the conducting plate at the bottom of the dielectric substrate. Owing to the thin dielectric substrate (usually less than one-quarter wavelength), a shunt inductance should also be added to the equivalent circuit when there is a metal-backed dielectric substrate immediately below the loop array. This qualitative equivalent circuit model for the DCR-MA is provided in Fig. 1b, where L_1, C_1, L_2, and C_2 are due to the DCRs and L_s accounts for the thin

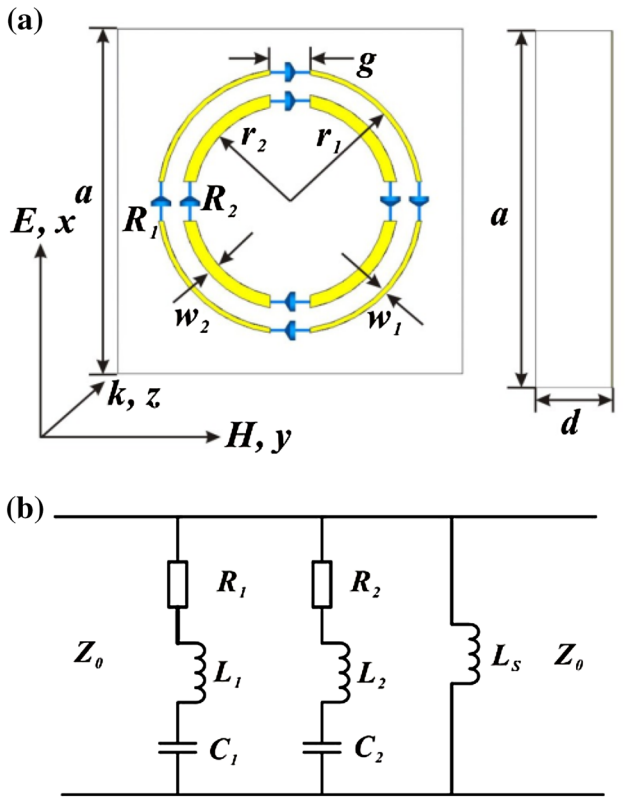

Fig. 1. (a) Front and right views of the DCR-MA unit cell. (b) Equivalent circuit model of the DCR-MA.

dielectric substrate backed by the copper plate. R_1 and R_2 are the equivalent resistances in each ring. From this equivalent circuit of the DCR-MA, it is clear that there are three resonant frequencies, which will result in a broad absorption bandwidth.

For the experiments, as shown in Fig. 2a, we first fabricated an MA sample with the optimized dimensions using conventional printed circuit board (PCB) technology, and then loaded lumped resistances R_1 and R_2 onto the DCR structure using welding technology. The final fabricated MA slab sample with lumped resistances had a unit cell of 14 mm × 14 mm with dimensions of 196 mm × 196 mm × 3 mm. Figure 2b shows a schematic diagram of the reflection measurement (free-space method).

The measurements were taken in an anechoic chamber. An Agilent PNA-X N5244A vector network analyzer and two broadband horn antennas were connected by a coaxial cable. Two antennas were used to emit and receive the EM wave. The distance between the sample and the antennas was set at about 2.5 m to avoid near-field effects. A bare aluminum board with the same size as the sample was used for calibration. The ratio between the reflection coefficients of the sample and the aluminum board was regarded as the reflection coefficient of the MA. The simulation and measurement results for the reflection by the DCR-MA are shown

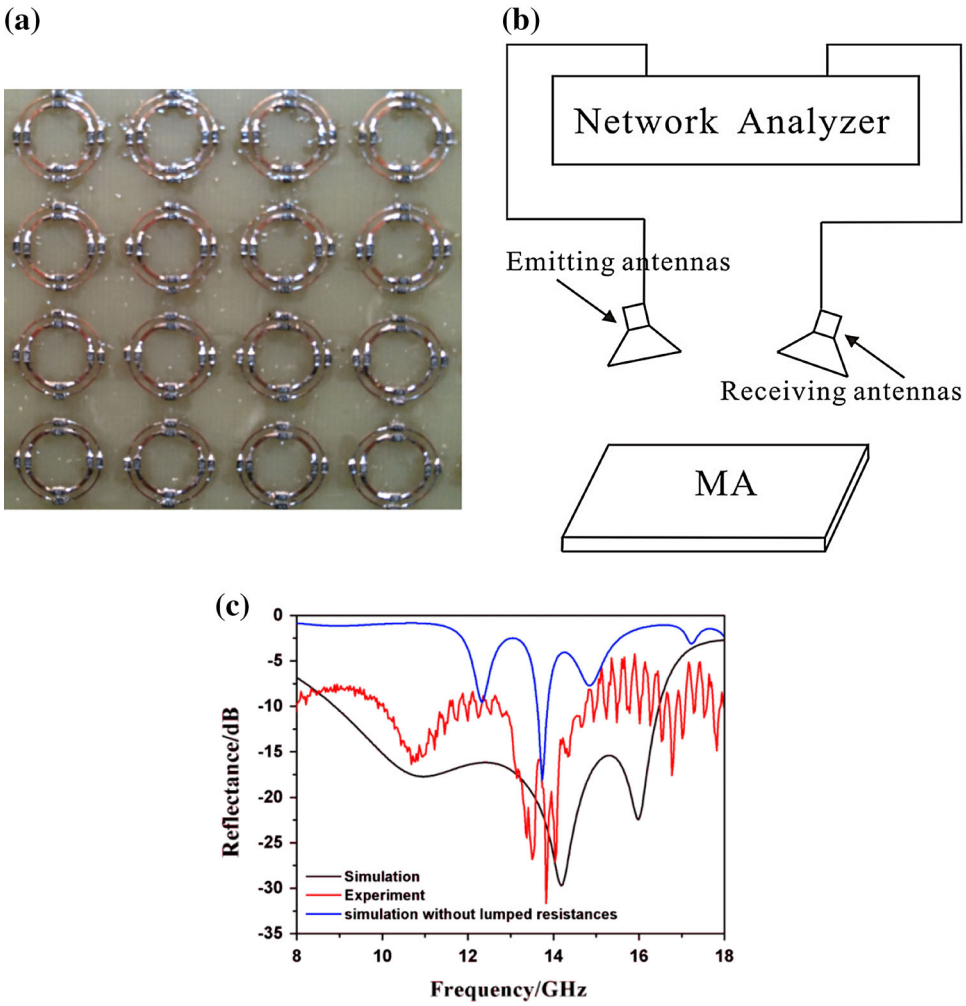

Fig. 2. (a) Portion of fabricated DCR-MA. (b) Schematic of reflection measurement system. (c) Simulation and experimental reflectances of DCR-MA and simulation result of DCR-MA without lumped resistances.

in Fig. 2c. It is obvious that the DCR-MA yields below −10 dB reflectance from about 8.87 GHz to 16.47 GHz in both the simulation and experimental results, and the fractional bandwidth (FBW) is about 60%. Additionally, the slight difference between the measured and simulated results (especially in the low frequency range) may be due to fabrication accuracy and measurement errors.

The polarization insensitivity was characterized by setting the polarization angle from 0° to 45°. It is sufficient to consider φ (0°, 45°) for normally incident EM waves. Figure 3 indicates the simulated absorption results for the DCR-MA for different polarization angles. One can easily see that the absorptivity remains nearly unchanged for different polarization angles, validating that this absorber is polarization insensitive at normal incidence.

For better understanding of the absorption mechanism by the DCR-MA, we investigated its

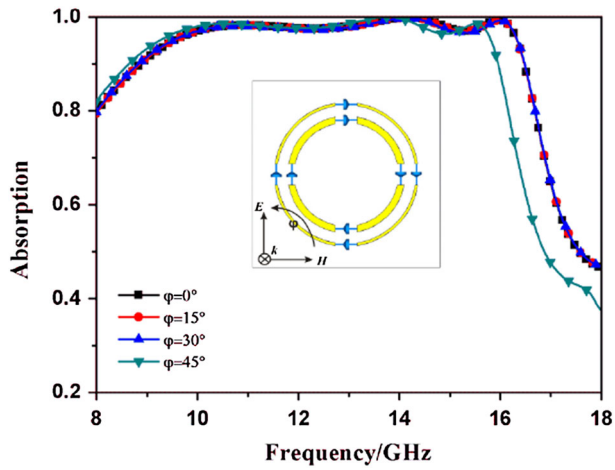

Fig. 3. Simulated absorption results for the DCR-MA for different polarization angles; inset shows the polarization angle and propagation direction.

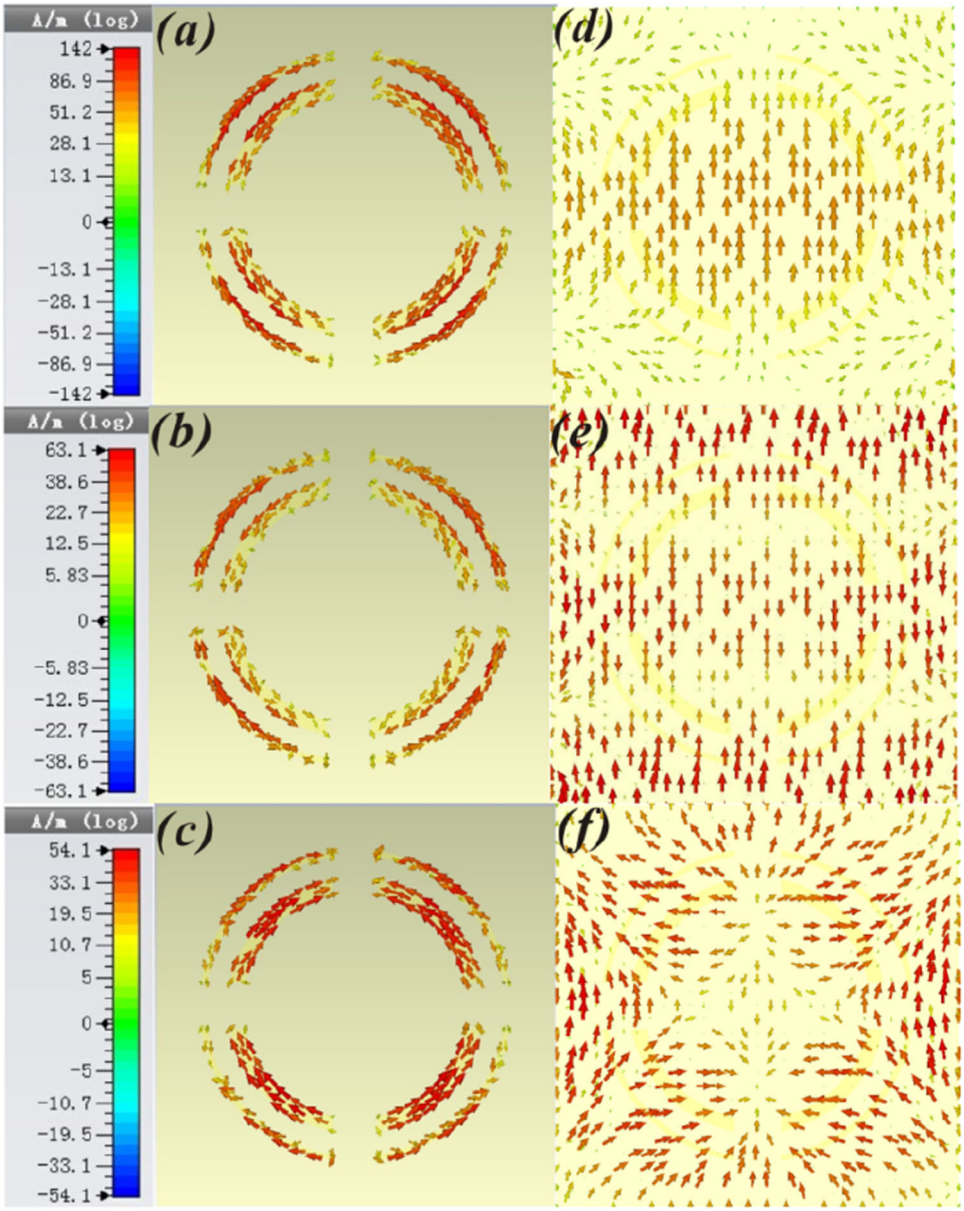

Fig. 4. Surface current distributions of the DCR structure: (a–c) front structure and (d–f) back ground plane at the corresponding absorption peaks of 12.32 GHz, 13.64 GHz, and 14.77 GHz.

absorptivity without the lumped resistances; the simulation results are shown in Fig. 2c. We simulated the surface current distributions of the absorber, as shown in Fig. 4a–f. The surface currents present a symmetric distribution at the absorption peaks, which is similar to the electric *LC* resonator. At these resonances, surface currents in the borderlines and gaps of the circle rings are stronger than in the in-plane case. Strong charge accumulation is produced along the electric field direction, resulting in strong electric resonance. At the same time, the direction of the surface currents in the front structure is nearly opposite to that in the continuous back metal plane, creating a magnetic flux that couples with the incident magnetic field. Additionally, the structure achieves two types of resonance resulting from coupling between the inner and outer circle rings. Therefore, the absorption of the designed structure is mainly due to local EM coupling resonance, as for conventional MAs. When the structure is loaded with the resistances, the surface current distributions are similar to this case, but become relatively complex and result in stronger EM coupling resonances. The equivalent *RLC* resonance circuit of the DCR-MA is shown in Fig. 1b. We can conclude that the three absorption peaks at the resonant frequencies of 12.32 GHz, 13.64 GHz, and 14.77 GHz can be mainly attributed

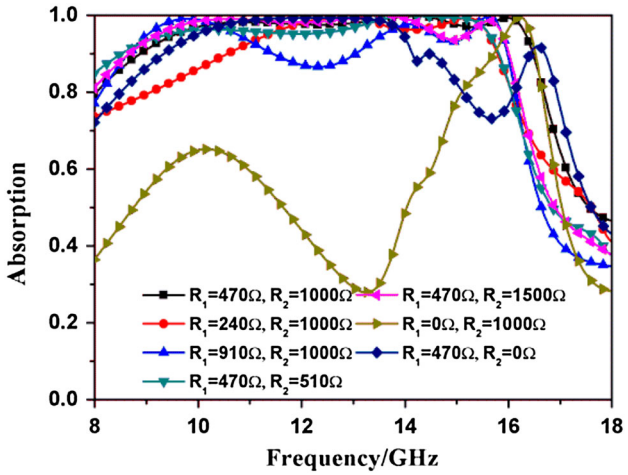

Fig. 5. Simulated absorption of DCR-MA with different lumped resistances.

to the DCR structure, and the broadband absorption of the proposed MA is due to both the lumped resistances and DCR structure.

To further examine the influence of the values of the lumped resistances on the absorption by the composite MA, we simulated the absorptivity of the DCR-MA with different lumped resistances, as shown in Fig. 5. One can see that the lumped parameters have optimum values and the low- and high-frequency resonances are caused by R_1 and R_2, respectively. These results further confirm that the bandwidth of the MA with only the DCRs can be greatly extended by loading with lumped resistances.

In practical applications, efficient absorbers are required not only to absorb as much radiation as possible but also be insensitive to the direction of incidence. Therefore, we also investigated the performance of the proposed absorber at various incidence angles. For the case of TE waves, depicted in Fig. 6a, broadband absorption performance was maintained to about 60°. The absorbance dropped sharply beyond 60° because the incident magnetic flux in the sandwich structure decreases with increasing incidence angle. For the TM case, shown in Fig. 6b, the stronger absorption band gradually splits with increasing incidence angle. This is due to the unchanged magnetic flux between the designed structure and the copper plane, which can provide strong magnetic resonance at all angles of incidence. However, the absorption is still greater than 50% when the incidence angle is below 60°. Additionally, with a 3-mm-thick substrate, the inductive impedance due to the metal-backed dielectric slab suffers stronger variation with increasing incidence angle.

SUMMARY AND DISCUSSION

In this work, a broadband MA based on DCRs loaded with lumped resistances was designed, simulated, and measured for analysis at microwave frequencies. The absorption results characterize the proposed MA at both normal and oblique incidence. The performance of the proposed MA, which has a very simple design, is compared with that of other similar MA structures in Table I. Most absorbers reported in the literature[15,16,19–22] use thick substrates over 5 mm, and some of them exhibit poor polarization independence and their incidence angle independence has not been explored. At the same time, many of these MA structures have a low FBW level. Although the proposed MA structure is just an extension of earlier publications,[15,16,19–22] its perfect broadband absorption, thin design, polarization independence, and simplicity represent important advantages. These significant properties are due to the combination of the electrical thickness, dielectric substrate, copper ground plane, *RLC* resonance, and EM interaction between the incident wave and absorber. In addition, this study deals with an interesting and challenging topic, since MAs have many present and prospective applications. Such

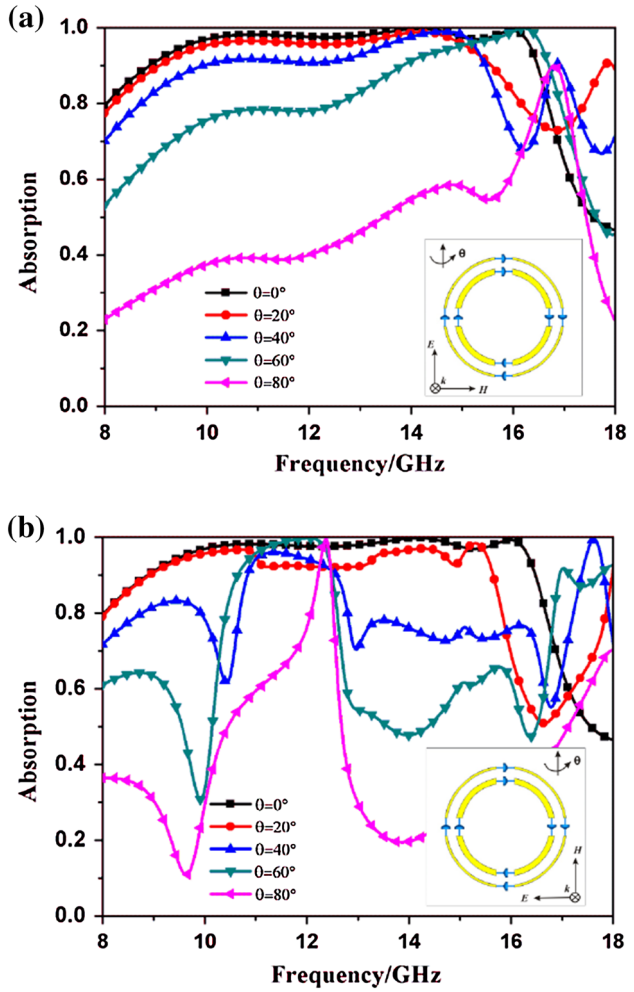

Fig. 6. Simulated absorption of DCR-MA at different incident angles for (a) TE and (b) TM wave; insets indicate the polarization and propagation directions of the incident wave.

Table I. Performance comparison with similar MAs

Reference	Thickness (mm)	Unit Cell Dimensions (mm)	Frequency Band (GHz)	FBW (%)	Polarization Independence	Incidence Angle Independence
This study	3	Double-circle rings 14 × 14	8.87–16.47	60.0	Yes	Below 40°
15	10	Double-square loops 40 × 40	1.0–5.0	50.0	Yes	Not discussed
16	6.5	Double U-shaped 10 × 6	7.7–18.0	Not calc.	No	Not discussed
19	6	Split-coin 40 × 40	3.1–5.6	55.0	Yes	Not discussed
20	0.2	ELC-SRR sandwich 30 × 30	2.05–2.75	Not calc.	No	Not discussed
21	10	Split-square coin 57 × 57	1.57–3.07	64.7	Yes	Not discussed
22	5	Split-coin 30 × 30	2.85–5.31	60.3	Yes	Not discussed

ELC-SRR electrically coupled LC split-ring resonator.

broadband and polarization-independent MAs could be useful for applications in future designs with the aim of improving angular stability.

CONCLUSIONS

We present an MA based on lumped resistances with a simple structure and ultrathin design, offering broadband absorption independent of polarization and incidence angle. Simulation and experimental results show that the proposed absorber has strong broadband absorption of above 90% from 8.87 GHz to 16.47 GHz and FBW of up to 60%. The absorption rates of the MA at different angles of incidence for TE and TM waves are investigated by simulation. In addition, the absorption mechanism is analyzed using an equivalent circuit model. The results show that the proposed absorber, which has the advantages of broadband absorption and a thin structure, is a promising candidate for use in stealth technology.

ACKNOWLEDGEMENTS

This work was supported by the special funds of the State Key Laboratory of Advanced Electromagnetic Engineering and Technology, Huazhong University of Science and Technology (Grant No. 2014ZZ001).

REFERENCES

1. N.I. Landy, S. Sajuyigbe, J.J. Mock, D.R. Smith, and W.J. Padilla, *Phys. Rev. Lett.* 100, 207402 (2008).
2. S. Bhattacharyya, S. Ghosh, and K.V. Srivastava, *J. Appl. Phys.* 114, 094514 (2013).
3. G.D. Wang, M.H. Liu, X.W. Hu, L.H. Kong, L.L. Cheng, and Z.Q. Chen, *Chin. Phys. B* 23, 017802 (2014).
4. L. Huang and H. Chen, *Prog. Electromagn. Res.* 113, 103 (2011).
5. X. Huang, H. Yang, S. Yu, J. Wang, M. Li, and Q. Ye, *J. Appl. Phys*. 113, 213516 (2013).
6. B. Wang, T. Koschny, and C.M. Soukoulis, *Phys. Rev. B* 80, 033108 (2009).
7. X. Shen, T.J. Cui, J. Zhao, H.F. Ma, X.W. Jiang, and H. Li, *Opt. Express* 19, 9401 (2011).
8. J. Zhao, Q. Cheng, J. Chen, M.Q. Qi, W.X. Jiang, and T.J. Cui, *New J. Phys*. 15, 043049 (2013).
9. H. Xiong, J.S. Hong, C.M. Luo, and L.L. Zhong, *J. Appl. Phys.* 114, 064109 (2013).
10. H.B. Zhang, L.W. Deng, P.H. Zhou, L. Zhang, D.M. Chen, H.Y. Chen, and L.J. Deng, *J. Appl. Phys.* 113, 013903 (2013).
11. Y.Z. Cheng, Y. Nie, X. Wang, and R.Z. Gong, *J. Appl. Phys.* 115, 042902 (2014).
12. F. Sakran, Y.Y. Neve-Oz, A. Ron, M. Golosovsky, D. Davidov, and A. Frenkel, *IEEE Trans. Antennas Propag.* 56, 2649 (2008).
13. F. Costa, A. Monorchio, and G. Manara, *IEEE Trans. Antennas Propag.* 58, 1551 (2010).
14. H.B. Zhang, P.H. Zhou, H.P. Lu, Y.Q. Xu, D.F. Liang, and L.J. Deng, *IEEE Trans. Antennas Propag.* 61, 976 (2013).
15. J. Yang and Z. Shen, *IEEE Antennas Wirel. Propag.* Lett. 6, 388 (2007).
16. Y.Z. Cheng, R.Z. Gong, Y. Nie, and X. Wang, *Chin. Phys. B* 21, 127801 (2012).
17. R.J. Langley and E.A. Parker, *Electron. Lett.* 18, 294 (1982).
18. R.J. Langley and E.A. Parker, *Electron. Lett.* 19, 675 (1983).
19. Y.Z. Cheng, Y. Wang, Y. Nie, R.Z. Gong, X. Xiong, and X. Wang, *J. Appl. Phys.* 111, 044902 (2012).
20. S. Gu, J.P. Barrett, T.H. Hand, B.I. Popa, and S.A. Cummer, *J. Appl. Phys.* 108, 064913 (2010).
21. C. Gu, S.B. Qu, Z.B. Pei, H. Zhou, Z. Xu, P. Bai, W.D. Peng, and B.Q. Lin, *Chin. Phys. Lett.* 27, 117802 (2010).
22. W.S. Yuan and Y.Z. Cheng, *Appl. Phys. A* 117, 1915 (2014).